Single-particle orbitals in liquid-helium drops

D. S. Lewart and V. R. Pandharipande
Department of Physics and Materials Research Laboratory, University of Illinois, Urbana, Illinois 61801

Steven C. Pieper
Physics Division, Argonne National Laboratory, Argonne, Illinois 60439-4843

(Received 27 July 1987; revised manuscript received 13 November 1987)

Drops containing 20 to 240 atoms of Bose liquid ^{4}He and Fermi liquid ^{3}He are studied by variational Monte Carlo methods as simple examples of correlated inhomogeneous quantum systems. In the present work we report wave functions of natural, quasiparticle, and mean-field orbitals in these drops. The wave functions of natural orbitals are determined by diagonalizing the one-particle density matrix. The condensate fraction and wave function in the Bose-liquid drops are calculated. The quasihole states are defined in the spirit of Landau's theory, and their wave functions are calculated from the overlaps between states containing N and $N-1$ atoms. In Bose-liquid drops the wave function of the quasihole orbital is similar to that of the condensate; however, in Fermi-liquid drops the quasihole wave functions are different from those of natural or mean-field orbitals. We find that a simple local-density approximation provides an accurate relation between the mean-field and quasihole wave functions for both Bose- and Fermi-liquid drops. The wave functions of natural orbitals are very localized and simple methods to construct them from mean-field wave functions are also discussed. The momentum distributions of atoms in the drops are calculated and compared with those of extended liquids. The deviations of the momentum distributions from mean-field distributions are also discussed.

I. INTRODUCTION

We have recently studied[1] the ground states of drops of Fermi liquid ^{3}He and Bose liquid ^{4}He with the variational Monte Carlo method. These drops provide simple examples of condensed states of ~ 100 Bose or Fermi particles that can be realistically studied at the microscopic level. It has not yet become possible to investigate neutral drops of helium liquids containing ~ 100 atoms in the laboratory; however, we hope that the present work is of interest in the fields of nuclear, small cluster, atomic, and molecular physics.

The variational wave functions used to study the ground states of liquid-helium drops containing more than 20 atoms have the form:

$$\Psi_v = \prod_{i<j\le N} f_2(r_{ij}) \prod_{i<j<k\le N} f_3(\mathbf{r}_{ij},\mathbf{r}_{ik})\Phi_v \ , \tag{1.1}$$

where f_2 and f_3 are two- and three-body correlation functions. In Bose drops the single-particle correlation is just a product:

$$\Phi_v = \prod_{i\le N} f_1(r_i) \ , \tag{1.2}$$

and in Fermi drops it is a product of determinants of the spin-up and of the spin-down atoms:

$$\Phi_v = \det[f_i(\mathbf{r}'_j)]\det[f_i(\mathbf{r}'_k)] \ . \tag{1.3}$$

The $f_i(\mathbf{r})$ $(1\le i\le N/2)$ are the lowest $N/2$ single-particle wave functions in a potential well; the subscript j $(1\le j\le N/2)$ denotes spin-up particles, while k $(N/2+1\le k\le N)$ denotes spin-down particles; and

$$\mathbf{r}'_i = \mathbf{r}_i + \sum_{j\,(\ne i)} \mathbf{r}_{ij}\eta(r_{ij}) \ , \tag{1.4}$$

where $\eta(r_{ij})$ is the backflow correlation function. It has been pointed out in Ref. 1 that because they are meant to be used with the two- and three-body correlations, the single-particle functions $f_i(\mathbf{r})$ do not by themselves provide a good description of single-particle properties, such as the density distribution.

Single-particle wave functions can be defined so as to reproduce a chosen observable property of the many-body system. Thus, there are many different ways to define single-particle wave functions. In the present work we consider three different single-particle wave functions called the natural orbitals, $\psi_i(r)$, the quasiparticle wave functions, $\chi_i(r)$, and the mean-field wave functions, $\phi_i(r)$. In extended liquids all these single-particle wave functions are plane waves due to translational invariance, but in a finite or inhomogeneous system they are generally different from each other.

The natural orbitals[2] are obtained by diagonalizing the one-particle density matrix:

$$\rho(\mathbf{r}_1,\mathbf{r}'_1) = N\int \Psi_0^*(\tau)\Psi_0(\mathbf{r}'_1,\tau'_1)d\tau'_1 \tag{1.5}$$

$$= \sum_i n_i\psi_i^*(\mathbf{r}_1)\psi_i(\mathbf{r}'_1) \ , \tag{1.6}$$

where n_i are the occupation probabilities of the states ψ_i, and we use the symbols $\tau=\mathbf{r}_1,\mathbf{r}_2,\ldots,\mathbf{r}_N$ and $\tau'_i=\mathbf{r}_1,\mathbf{r}_2,\ldots,\mathbf{r}_{i-1},\mathbf{r}_{i+1},\ldots,\mathbf{r}_N$. Here Ψ_0 is the exact ground-state wave function; in practice it is approximat-

ed by the variational Ψ_v. We have calculated the natural orbitals ψ_i in Bose- and Fermi-liquid drops containing 70 atoms. The methods and results are presented in Sec. III. The density matrix $\rho(\mathbf{r},\mathbf{r}')$ also gives the distribution of atoms in coordinate and momentum space:

$$\rho(\mathbf{r})=\rho(\mathbf{r},\mathbf{r})=\sum_i n_i \mid \psi_i(\mathbf{r}) \mid^2 , \tag{1.7}$$

$$\tilde{\rho}(\mathbf{k})=\frac{1}{(2\pi)^3}\int e^{i\mathbf{k}\cdot(\mathbf{r}-\mathbf{r}')}\rho(\mathbf{r},\mathbf{r}')d^3r\,d^3r' , \tag{1.8}$$

$$=\sum_i n_i \mid \tilde{\psi}_i(\mathbf{k}) \mid^2 , \tag{1.9}$$

where

$$\tilde{\psi}_i(\mathbf{k})=\frac{1}{(2\pi)^{3/2}}\int e^{-i\mathbf{k}\cdot\mathbf{r}}\psi_i(\mathbf{r})d^3r . \tag{1.10}$$

The $\rho(\mathbf{r})$ of helium drops is given in Ref. 1, and the $\tilde{\rho}(\mathbf{k})$ is discussed in Sec. IV. The normalization is such that their integral is the number of atoms in the drop.

The quasiparticle wave functions $\chi_h(r)$ of hole states are obtained from the expression

$$\chi_h(\mathbf{r}_1)\propto\int\Psi_h^*(\tau_1')\Psi_0(\tau)d\tau_1' , \tag{1.11}$$

where Ψ_h are low-energy single-hole states of drops having $N-1$ particles. We have approximated the Ψ_h as follows:

$$\Psi_h=\prod_{2\le i<j\le N} f_2(r_{ij})\prod_{2\le i<j<k\le N} f_3(\mathbf{r}_{ij},\mathbf{r}_{ik})\Phi_h . \tag{1.12}$$

In Bose-liquid drops Φ_h is obtained by omitting the factor $f_1(r_1)$ in Eq. (1.2) and making a small shift of the other $f_1(r_i)$, while in Fermi-liquid drops it is obtained by omitting the row for particle 1, and the column for state f_h in the first determinant in Eq. (1.3). When the excitation energy of the single-particle or single-hole state is large, it acquires a large width due to its coupling to more complicated states. Hence, the quasiparticle wave functions are more meaningful for the low-energy single-particle or single-hole states. These wave functions are discussed in Sec. V.

In the mean-field model the ground-state wave function is approximated for Bose-liquid drops as

$$\Phi_{MF}=\prod_{i\le N}\phi_0(\mathbf{r}) , \tag{1.13}$$

and for Fermi drops as

$$\Phi_{MF}=\det[\phi_i(\mathbf{r}_j)]\det[\phi_i(\mathbf{r}_k)] . \tag{1.14}$$

We choose to obtain the single-particle wave functions $\phi_i(\mathbf{r})$ by reproducing the one-particle density $\rho(\mathbf{r})$ as discussed in Sec. II. The last section includes a pedagogical discussion of the one-particle Green's function in finite systems.

Throughout this paper, lengths are expressed in terms of σ ($1\sigma=2.556$ Å) and momenta in inverse σ. Single-particle wave functions with vector arguments $[\phi_i(\mathbf{r})]$ are normalized such that

$$\int \mid \phi_i(\mathbf{r}) \mid^2 d^3r=1 , \tag{1.15}$$

whereas the absence of a vector argument implies a radial function with normalization:

$$\int \mid \phi_i(r) \mid^2 r^2\,dr=1 . \tag{1.16}$$

II. MEAN-FIELD SINGLE-PARTICLE ORBITALS

The rotational invariance of the Hamiltonian implies that the total angular momentum L and its projection M are good quantum numbers. We note that in the Hamiltonian of Ref. 1, the interaction between ^{3}He atoms is independent of the spin of the atoms, and hence for the most part the spin can be ignored. The ground states of Bose systems have a nodeless wave function; thus they have $L=M=0$. The single-particle orbitals in these spherically symmetric drops have l and m as good quantum numbers. In the mean-field model all N particles are in the $n=l=m=0$ state ϕ_{1s} and by requiring that this model reproduce the true density distribution $\rho(r)$ we obtain

$$\phi_{1s}(\mathbf{r})=[\rho(r)/N]^{1/2} \tag{2.1}$$

in Bose-liquid drops. The other mean-field orbitals ϕ_{nl} having $n>0$ or $l>0$ are not discussed here.

The shell structure of Fermi-liquid ^{3}He drops has been discussed by Stringari.[3] The drops studied in Ref. 1 have values of N that correspond to closed shells. The ground states of these drops also have $L=M=0$ as well as total spin $S=0$. If we assume that the mean-field potential is a local function $V(r)$, then the ϕ_i can be obtained from the Schrödinger equation

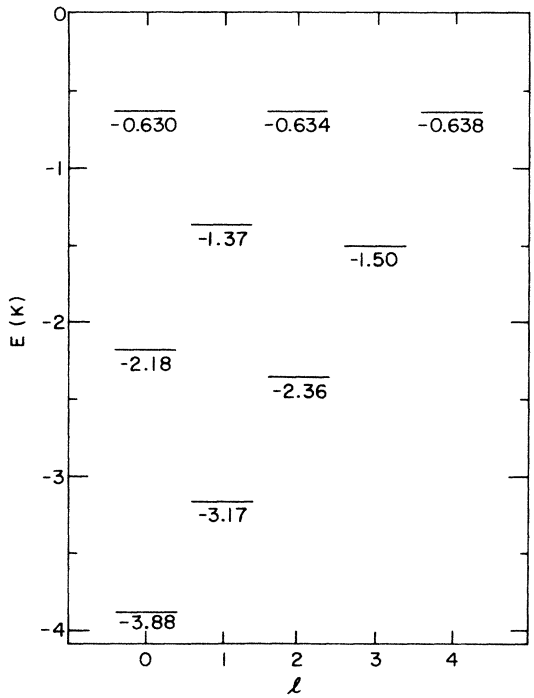

FIG. 1. The energies of single-particle states in the single-particle potential $V(r)$ shown in Fig. 2.

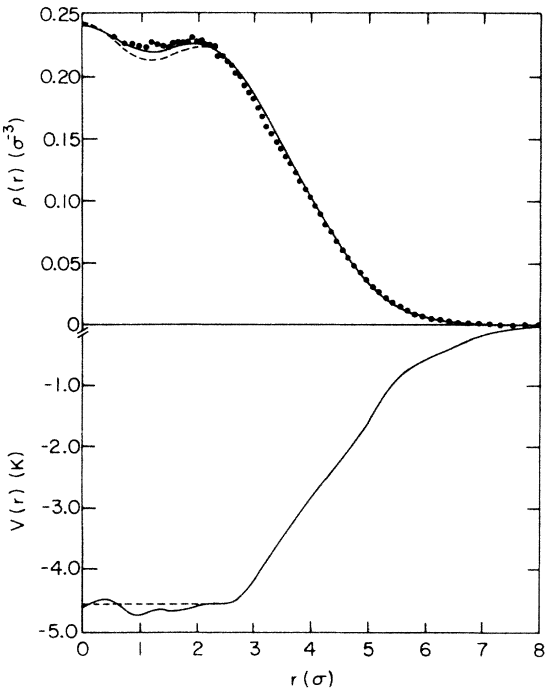

FIG. 2. The density distribution $\rho(r)$ (curves) obtained by filling the lowest 70 states in the single-particle potential $V(r)$, compared with the $\rho(r)$ obtained in Ref. 1 for the $N=70$ liquid ^{3}He drop by a Monte Carlo calculation with Ψ_v (data points). The lower panel shows $V(r)$. The solid curves are for the $V(r)$ used in this work and the dashed curves are for a flat-bottom well.

$$\left[-\frac{\hbar^2}{2m}\nabla^2+V(r)\right]\phi_i(\mathbf{r})=e_i\phi_i(\mathbf{r})\ ; \tag{2.2}$$

the potential $V(r)$ is chosen so that the mean-field model density equals the true density $\rho(r)$. Most of the present work is focused on the $N=70$ Bose- and Fermi-liquid drops. The mean-field energy eigenvalues e_i for the Fermi-liquid $N=70$ drop are shown in Fig. 1. The potential $V(r)$ and the density distribution $\rho(r)$ are shown in Fig. 2. Note that the potential has oscillations that are out of phase with those of the $\rho(r)$. These oscillations reduce the shell fluctuations in $\rho(r)$. A $V(r)$ with a flat bottom yields a $\rho(r)$ that has too much shell fluctuation as illustrated by the dashed curve in Fig. 2.

In general, and in Hartree-Fock theory in particular, the mean-field potential is a nonlocal function $V(\mathbf{r},\mathbf{r}')$, and

$$-\frac{\hbar^2}{2m}\nabla^2\phi_i(\mathbf{r})+\int V(\mathbf{r},\mathbf{r}')\phi_i(\mathbf{r}')d^3r'=e_i\phi_i(\mathbf{r})\ . \tag{2.3}$$

In this case there is no unique one-to-one correspondence between $\rho(\mathbf{r})$ and the $\phi_i(\mathbf{r})$. We have not studied the ambiguities in the $\phi_i(\mathbf{r})$ due to the nonlocality of $V(\mathbf{r},\mathbf{r}')$.

III. NATURAL ORBITALS

A. Calculation of natural orbitals

The drops being considered here are spherically symmetric and thus the one-particle density matrix may be expanded as

$$\rho(\mathbf{r}_1,\mathbf{r}_1')=\sum_l\frac{2l+1}{4\pi}P_l(\hat{\mathbf{r}}_1\cdot\hat{\mathbf{r}}_1')\rho_l(r_1,r_1')\ , \tag{3.1}$$

where $P_l(x)$ is a Legendre function and

$$\rho_l(r_1,r_1')=N\int\Psi_v^*(\tau)P_l(\hat{\mathbf{r}}_1\cdot\hat{\mathbf{r}}_1')\times\Psi_v(\mathbf{r}_1',\tau_1')d\Omega_1d\tau_1'\Big/\int|\Psi_v(\tau)|^2d\tau\ . \tag{3.2}$$

In Eq. (3.2) $d\Omega_1$ denotes an integration over the directions of $\mathbf{r}_1$, and $\hat{\mathbf{r}}_1'$ may be any fixed direction. We evaluate $\rho_l(r,r')$ on grids of l values of r and r' values (the same grid is used for both r and r') by making a Metropolis random walk in the space τ with the walk controlled by $|\Psi_v(\tau)|^2$. At each configuration, we determine the bin that $|\mathbf{r}_1|$ is in and evaluate

$$\Psi_v(\mathbf{r}_1',\tau_1')/\Psi_v(\tau)P_l(\hat{\mathbf{r}}_1\cdot\hat{\mathbf{r}}_1') \tag{3.3}$$

for all values of l and r_1' and fixed $\hat{\mathbf{r}}_1'$. The average value of expression (3.3) gives $\rho_l(r_1',r_1)$. Because $\rho_l(r,r')$ is independent of the direction $\hat{\mathbf{r}}_1'$, we can evaluate (3.3) for different directions and average these values together to reduce the statistical fluctuations. We used six directions, $\pm\hat{\mathbf{x}}$, $\pm\hat{\mathbf{y}}$, $\pm\hat{\mathbf{z}}$, for each value of r_1'. Furthermore, because $\rho_l(r,r')$ is independent of which particle is moved in Eq. (3.2), we calculate and average over all of them.

The one-particle density matrix is, of course, symmetric,

$$\rho_l(r,r')=\rho_l(r',r)\ , \tag{3.4}$$

but the method outlined above is not manifestly symmetric. We verified that, within statistical errors, $\rho_l(r,r')=\rho_l(r',r)$ and then we symmetrized $\rho_l(r,r')$ by forming a weighted average of $\rho_l(r,r')$ and $\rho_l(r',r)$.

The spherical symmetry of the drops allows us to write the natural orbitals of Eq. (1.6) as

$$\psi_i(\mathbf{r})=\psi_{nl}(r)Y_{lm}(\hat{\mathbf{r}})\ . \tag{3.5}$$

The radial orbitals and their occupation numbers are then the eigenvectors and eigenvalues of $\rho_l(r,r')$:

$$\rho_l(r,r')=\sum_n n_{nl}\psi_{nl}(r)\psi_{nl}(r')\ . \tag{3.6}$$

We will often show results for the radial functions $u_{nl}(r)$:

$$u_{nl}(r)=r\psi_{nl}(r)\ . \tag{3.7}$$

We have extracted these eigenvectors and the corresponding eigenvalues by two methods. In the first, we directly diagonalize the matrix

$$\rho_{l,ij}=\rho_l(r_i,r_j)\ . \tag{3.8}$$

This method has the advantage of introducing no bias about the functional form of $u_{nl}(r)$ but has the disadvantage, due to the relatively large sampling errors in $\rho_l(r,r')$ for small r or r', of not producing radial functions with the correct r^{l+1} behavior at the origin. The statistical errors in the so-extracted $u_{nl}(r)$ also make it difficult to compute the Fourier transforms $\tilde{u}_{nl}(k)$.

In the second method we expand the $\rho_l(r,r')$ in terms of the oscillator functions $h_{nl}(r)$:

$$M^l_{ij}=\int\int h_{il}(r)\rho_l(r,r')h_{jl}(r')dr\,dr' \tag{3.9}$$

for $i,j\leq I$ with I less than the number of points on the grid used to compute $\rho_l(r,r')$. The eigenvectors of M^l may be used to construct $u_{nl}(r)$ with the correct behavior at the origin.

Table I shows the eigenvalues of $\rho_{l=0}(r,r')$ for the 70-atom ^{3}He drop computed by these methods. (Note that the eigenvalues are twice the occupation numbers.) We used a 28-element grid to compute $\rho_l(r,r')$ so method 1 gives us 28 eigenvalues. However, because of the statistical errors in $\rho_0(r,r')$, eleven of these are negative (the sum of the negative eigenvalues is -0.01). Column 4 of Table I shows the ten largest eigenvalues. Columns 1 to 3 show the corresponding eigenvalues computed using 11, 16, and 21 oscillator functions, respectively. The first, third, and fifth eigenvectors computed by method 1 (symbols) and with 11 and 16 oscillator functions (curves) are shown in Fig. 3. The curves for 21 oscillator functions are indistinguishable from those for 16 functions. It can be seen that the two methods are in good agreement and that eigenvalues down to ~ 0.01 are probably reliable. In the rest of the paper we present results obtained using 16 oscillator functions.

B. Natural orbitals of the $N=70$ Liquid ^{4}He Drop

Some of the s-wave natural orbitals of the 70-particle Bose-liquid ^{4}He drop are shown in Fig. 4 along with the $1s$ mean-field orbital. We note that all the natural orbitals are confined in the region where $\rho(\mathbf{r})\neq 0$. Equation (1.7) implies that the $\psi_i(\mathbf{r})$ are zero where $\rho(\mathbf{r})=0$. The occupation numbers of the natural orbitals are given in Table II. A significant fraction (36%) of the particles are condensed in the $1s$ natural orbital of the 70-particle drop, as against $\sim 10\%$ in the extended liquid. The dependence of the condensate fraction on the number of particles is discussed in Sec. IV.

The partial density of the particles condensed in the $1s$ natural orbital is called the condensate density,

$$\rho_c(r)=n_{1s}\,|\,\psi_{1s}(\mathbf{r})\,|^2\,, \tag{3.10}$$

and it is compared with the total density $\rho(r)$ in Fig. 5. We note that at the center of the drop $\rho_c(0)\simeq 0.1\rho(0)$, as expected from studies of the extended liquid.

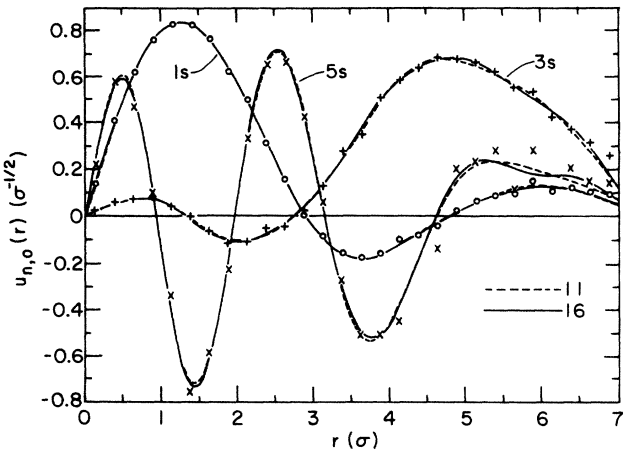

FIG. 3. The $1s$, $3s$, and $5s$ natural orbitals of the 70-atom ^{3}He drop obtained with 11 (dashed curves) and 16 (solid curves) oscillator functions. The symbols show the eigenfunctions obtained by diagonalizing in coordinate space.

TABLE I. Eigenvalues of $\rho_{l=0}(r,r')$ for 70 ^{3}He atoms. Columns 1–3 show the eigenvalues computed in an oscillator basis containing, respectively, the first 11, 16, and 21 oscillator functions. The last column shows the eigenvalues resulting from a direct diagonalization of $\rho_{l=0}(r,r')$ on a 28×28 point grid in r space. In all cases only the first ten eigenvalues are shown.

n	$I=11$	$I=16$	$I=21$	28×28
1	1.0801	1.0803	1.0804	1.0816
2	1.2565	1.2575	1.2580	1.2600
3	1.6963	1.6987	1.6996	1.7066
4	0.1476	0.1477	0.1477	0.1495
5	0.0782	0.0784	0.0784	0.0799
6	0.0376	0.0378	0.0382	0.0427
7	0.0160	0.0197	0.0197	0.0232
8	0.0007	0.0065	0.0067	0.0084
9	4.0×10^{-5}	0.0010	0.0022	0.0071
10	-1.0×10^{-6}	0.0004	0.0010	0.0044

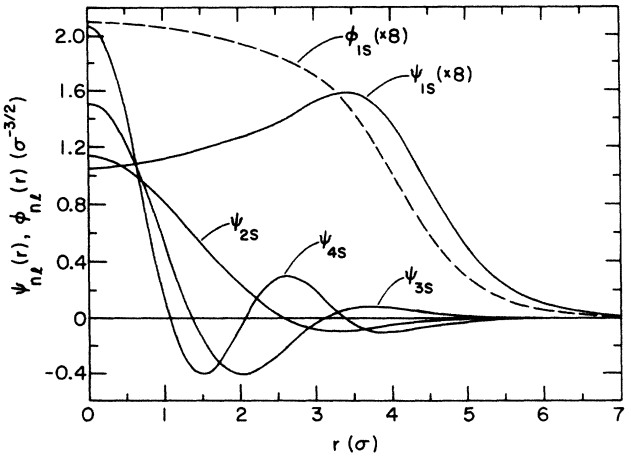

FIG. 4. The s-wave natural orbitals ($1s$ to $4s$) of the 70-particle Bose-liquid ^{4}He drop (solid lines). The dashed curve shows the $1s$ mean-field orbital. The ψ_{1s} and ϕ_{1s} have been multiplied by 8.

TABLE II. Occupation numbers of natural orbitals of the $N=70$ Bose-liquid ^{4}He drop.

n,l	$n_{n,l}$	n,l	$n_{n,l}$	n,l	$n_{n,l}$
$1s$	25.33	$1h$	0.24	$1k$	0.104
$1p$	0.49	$2f$	0.22	$2i$	0.086
$1d$	0.44	$3p$	0.22	$3g$	0.078
$2s$	0.44	$1i$	0.19	$4d$	0.077
$1f$	0.37	$2g$	0.17	$5s$	0.100
$2p$	0.35	$3d$	0.16	$1l$	0.063
$1g$	0.30	$4s$	0.19	$2j$	0.060
$2d$	0.28	$1j$	0.14	$3h$	0.046
$3s$	0.30	$2h$	0.12	$4f$	0.049
		$3f$	0.11	$5p$	0.046
		$4p$	0.11		

In Bose-liquid drops the $1s$ natural orbital can be well approximated as follows:

$$\psi_{1s}(\mathbf{r}) \simeq A[1-0.68\rho(r)/\rho_0]\phi_{1s}(\mathbf{r}) \simeq A[1-0.68\rho(r)/\rho_0]\sqrt{\rho(r)/N} \ , \quad (3.11)$$

where A is a normalization constant and ρ_0 is the equilibrium density of liquid ^{4}He ($0.365\sigma^{-3}$). The wave function obtained from this approximation is practically indistinguishable from the $\psi_{1s}(r)$ in Fig. 4. The factor multiplying $\sqrt{\rho(r)/N}$ in Eq. (3.11) can be interpreted as $\sqrt{n_0[\rho(r)]}$, where $n_0(\rho)$ is the condensate fraction in liquid ^{4}He at density ρ, from the argument given in the next paragraph. Since extended liquid at $\rho<\rho_0$ is unstable, only $n_0(\rho)$ for $\rho\geq\rho_0$ has been studied.[4] In Fig. 6 we show that the function $(1-0.68\rho/\rho_0)$ provides a continuation of $\sqrt{n_0(\rho)}$ for $\rho<\rho_0$.

Consider an inhomogeneous Bose system with a density distribution $\rho(\mathbf{r})$. In mean-field theory, all the particles occupy the state $\phi_0(\mathbf{r})=\sqrt{\rho(\mathbf{r})/N}$. In reality, a certain fraction of the particles are condensed in the natural orbital $\psi_0(\mathbf{r})$. Now let us pretend that the inhomogeneous system is a large tank of liquid ^{4}He, with an external potential applied to the $x>0$ half such that the density distribution of the liquid in this tank is given by

$$\rho(\mathbf{r})=\begin{cases}\rho_L \ , & x\ll 0\\ \rho_R \ , & x\gg 0 \ .\end{cases} \quad (3.12)$$

(3.13)

Now the density of particles having momenta $k\sim 0$ at $x\ll 0$ is given by $n_0(\rho_L)\rho_L$, while for that at $x\gg 0$ it is $n_0(\rho_R)\rho_R$. Thus we have

$$N_c\psi_0^2(\mathbf{r})=\begin{cases}n_0(\rho_L)\rho_L \ , & x\ll 0 \quad (3.14)\\ n_0(\rho_R)\rho_R \ , & x\gg 0 \ , \quad (3.15)\end{cases}$$

where N_c is the number of particles condensed in the natural orbital ψ_0. This implies that when $\rho(\mathbf{r})$ is a slowly varying function of $\mathbf{r}$, the natural orbital $\psi_0(\mathbf{r})$ is approximately given by

$$\psi_0(\mathbf{r})\simeq A\sqrt{n_0[\rho(\mathbf{r})]}\sqrt{\rho(\mathbf{r})/N}=A\sqrt{n_0[\rho(\mathbf{r})]}\phi_0(\mathbf{r}) \ . \quad (3.16)$$

Equation (3.16) can be considered as a local-density approximation (LDA) for the condensate natural orbital. It is a good approximation in all the Bose-liquid drops ($N=20$–240) studied in this work.

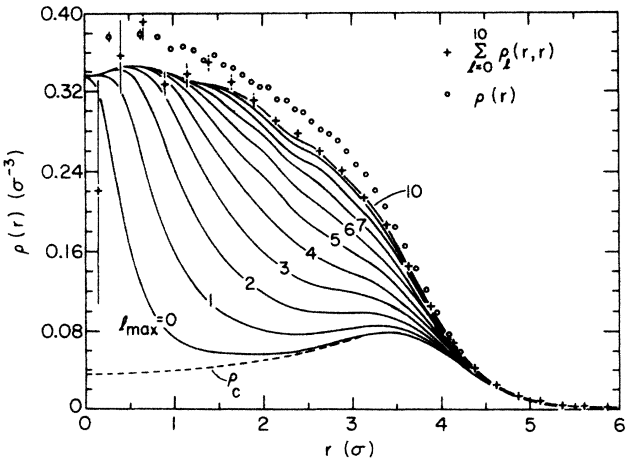

FIG. 5. The density $\rho(r)$ of the 70-atom ^{4}He drop (dots with error bars) from Ref. 1. The curves show the cumulative contributions of the natural orbitals up to a given l_{max} as obtained from the oscillator expansions. The crosses and error bars show the sum of $\rho_l(r,r)$ for l up to 10 and are to be compared with the uppermost curve. The dashed curve is the condensate contribution $\rho_c(r)$.

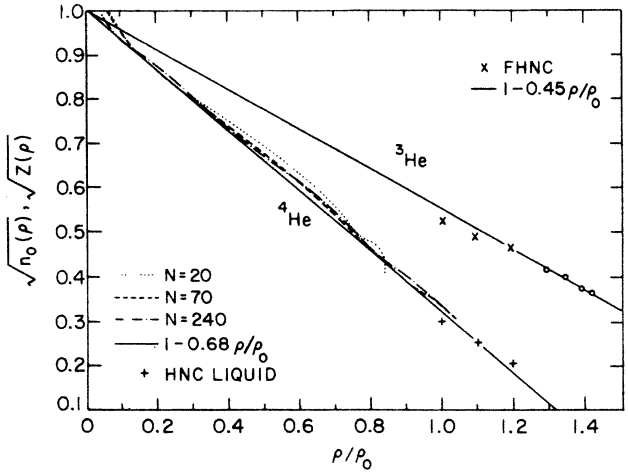

FIG. 6. Condensate amplitudes $\sqrt{n_0}$ as a function of density for liquid ^{4}He (lower curves and symbols) and the $\sqrt{z(\rho)}$ for liquid ^{3}He (upper line and symbols). The solid lines are the approximations $n_0(p)=(1-0.68\rho/\rho_0)^2$ (^{4}He) and $Z(\rho)=(1-0.45\rho/\rho_0)^2$ (^{3}He). The plus signs are from Ref. 4, the $\times$'s are from Ref. 5, and the circles are obtained by assuming that the experimental effective mass (Ref. 8) is given by $0.8/Z$ (Ref. 5). The ratio $\chi_{1s}(r)/\sqrt{\rho(r)}$, as described in the text, is shown for the 20-atom (dotted), 70-atom (dashed), and 240-atom (dot-dash) ^{4}He drops.

In the LDA the number of particles in the condensate is given by

$$n_{1s}=\int n_0[\rho(\mathbf{r})]\rho(\mathbf{r})d^3r \simeq \int [1-0.68\rho(\mathbf{r})/\rho_0]^2\rho(\mathbf{r})d^3r \ . \quad (3.17)$$

The n_{1s} estimated from this is 26.0 in the $N=70$ drop, as compared to 25.3 obtained by diagonalizing the density matrix. In this approximation the normalization A of $\psi_{1s}(\mathbf{r})$ [Eq. (3.11)] is simply $\sqrt{N/n_{1s}}$.

The number of particles that are not in the condensate and that have a given angular momentum l,

$$N_l=(2l+1)\sum_n n_{nl}(1-\delta_{n1}\delta_{l0}) \ , \quad (3.18)$$

are shown in Table III. The sum of n_{1s} and the N_l for $l\leq 10$ is 65.3, which implies that ~ 4.7 particles have $l>10$. The partial contributions,

$$\rho_l(r)=(2l+1)\sum_n n_{nl}(1-\delta_{n0}\delta_{l0})\,|\,\psi_{nl}(\mathbf{r})\,|^2 \ , \quad (3.19)$$

to the $\rho(r)$ are shown in Fig. 5, and the sum of $\rho_c(r)$ and $\rho_l(r)$ for $l\leq 10$ is compared with the total $\rho(r)$. The error bars shown for $\sum_{l=0}^{10}\rho_l(r,r)$ indicate that the deviations at small r are most likely due to sampling errors; the omitted contributions for $l>10$ are most significant for $1.5\sigma\leq r\leq 3.5\sigma$.

C. Natural orbitals of the $N=70$ Liquid ^{3}He Drop

In the mean-field theory of Fermi-liquid drops, the lowest N mean-field orbitals are occupied with unit probability, while the others are empty. In correlated normal (as against superfluid) Fermi systems there are also N orbitals with occupation probabilities that are significantly larger than those for the others. These are called the hole-state orbitals while the others are called particle orbitals. We first discuss the hole orbitals.

The wave functions of natural s, p, d, f, and g hole orbitals are compared with those of the mean-field orbitals in Figs. 7 and 8. We note that there is only one hole orbital for the $l=3$ ($1f$) and 4 ($1g$) states, and that for the $l=3$ and 4 hole states the natural and mean-field wave functions are qualitatively similar in the sense that they do not have radial nodes. In contrast there are two p ($1p$ and $2p$) and two d ($1d$ and $2d$) hole orbitals. The conventional mean-field $1p$ and $1d$ orbitals are nodeless while the $2p$ and $2d$ orbitals have one radial node; in contrast, the $1p$, $1d$, $2p$, and $2d$ natural orbitals have all one radial node. Similarly, the mean-field $1s$, $2s$, and $3s$ orbitals have zero, one, and two nodes, while the natural $1s$, $2s$, and $3s$ orbitals have two nodes each. The natural orbitals are much more localized than the mean-field orbitals, and we adopt a convention under which the orbital localized closest to $r=0$ has radial quantum number 1.

The occupation numbers of the orbitals are given in Table IV. The hole-state orbitals have significantly larger occupation probabilities than the particle states. The hole orbitals localized at small values of r ($1s$, for example), where the density is close to the equilibrium density of liquid ^{3}He ($0.277\sigma^{-3}$), have occupation probabilities of

TABLE III. Number of particles having a given angular momentum for the 70-atom ^{4}He drop. The number of particles in the condensate is shown separately.

l	N_l	
Condensate	25.33	26.46
0	1.13	
1	3.74	
2	5.06	
3	5.51	
4	5.55	
5	4.92	
6	4.20	
7	3.63	
8	2.98	
9	1.97	
10	1.32	
Total	65.34	

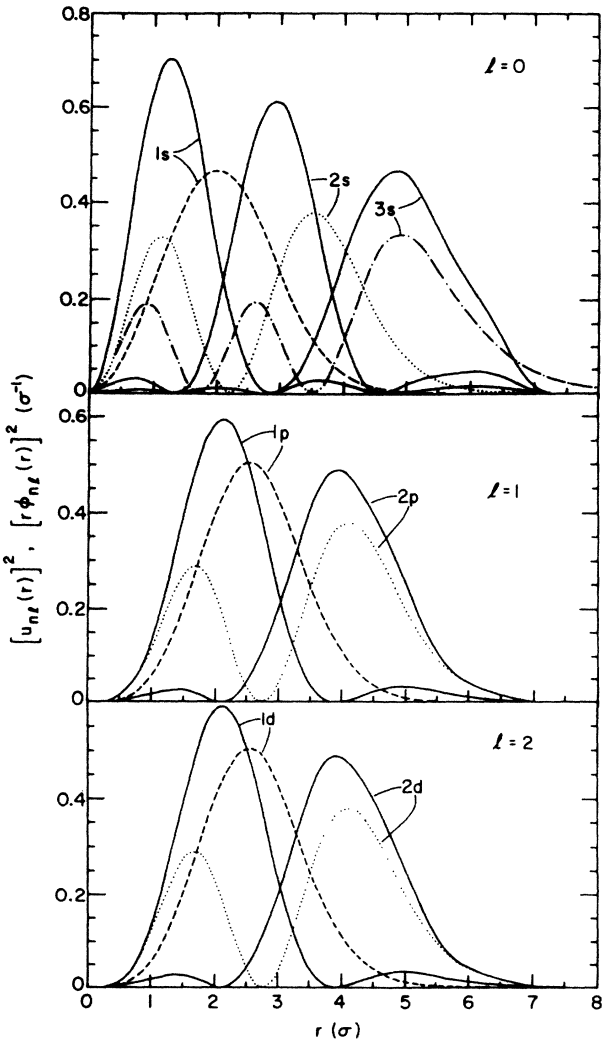

FIG. 7. The $1s$, $2s$, and $3s$ natural (solid lines) and mean-field (dashed, dotted, and dot-dash lines) orbitals in the 70-particle liquid ^{4}He drop. The figure shows $(u_{nl})^2$ and $(r\phi_{nl})^2$.

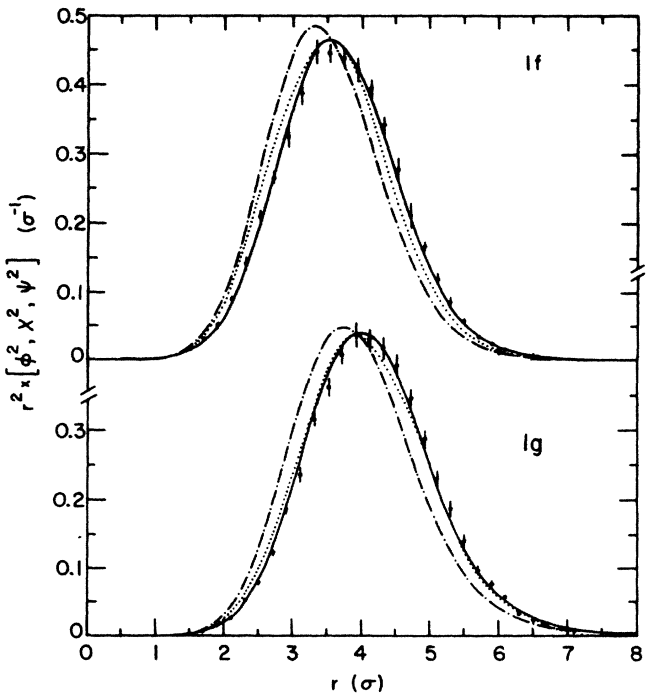

FIG. 8. The $\chi(r)$ (error bars), $\phi(r)$ (dot-dash), $\psi(r)$ (dotted), and LDA [Eq. (5.15)] for $\chi(r)$ (solid curve), for the $1f$ (upper curves) and $1g$ (lower curves). The figure shows $r^2\chi^2$, $r^2\psi^2$, and $r^2\phi^2$.

~ 0.5 that are typical for the hole states ($k < k_F$) of the liquid.[5] The hole orbitals localized at the surface ($3s$, for example) have much larger occupation probabilities because they are at much lower density.

It is obvious that when there is more than one hole state for a set of angular momentum quantum numbers l,m and spin projection σ_z, the natural orbitals are qualitatively different from conventional mean-field orbitals. However, it is well known in the mean-field theory that we can make any orthogonal linear combination of the mean-field hole orbitals without changing the mean-field density matrix $\rho(\mathbf{r},\mathbf{r}')$. Let $\phi_i'(r)$ denote localized mean-field orbitals. These are obtained by the following construction illustrated for p orbitals:

TABLE IV. Occupation numbers of natural orbitals of the $N=70$ Fermi-liquid ^{3}He drop.

n,l	$n_{n,l}$	n,l	$n_{n,l}$	n,l	$n_{n,l}$
$1s$	0.54	$1h$	0.059	$1k$	0.024
$1p$	0.58	$2f$	0.074	$2i$	0.022
$1d$	0.60	$3p$	0.081	$3g$	0.028
$2s$	0.63	$1i$	0.048	$4d$	0.038
$1f$	0.69	$2g$	0.062	$5s$	0.039
$2p$	0.77	$3d$	0.071	$1l$	0.018
$1g$	0.75	$4s$	0.074	$2j$	0.016
$2d$	0.84	$1j$	0.034	$3h$	0.013
$3s$	0.85	$2h$	0.033	$4f$	0.019
		$3f$	0.039	$5p$	0.022
		$4p$	0.045		

$$\phi_{1p}'(r)=\cos(\theta)\phi_{1p}(r)+\sin(\theta)\phi_{2p}(r)\ , \tag{3.20}$$

$$\phi_{2p}'(r)=-\sin(\theta)\phi_{1p}(r)+\cos(\theta)\phi_{2p}(r)\ . \tag{3.21}$$

The angle θ is chosen to maximize the peak heights of $(r\phi_i')^2$:

$$\frac{\partial}{\partial\theta}\{\max_r[r\phi_{1p}'(r)]^2+\max_r[r\phi_{2p}'(r)]^2\}=0\ . \tag{3.22}$$

The s-wave localized mean-field orbitals are compared with the natural hole orbitals in Fig. 9. They are obviously closer to the natural orbitals than the conventional mean-field orbitals. The agreement between localized mean-field and natural orbitals for the p and d waves is equally good.

The density matrix is not diagonal in the basis of mean-field orbitals. For example, the matrix elements for s-wave hole states are

$$\langle\phi_{n0}\,|\,\rho\,|\,\phi_{n'0}\rangle=\begin{bmatrix}0.59 & -0.058 & 0.0091\\ -0.058 & 0.66 & -0.115\\ 0.0091 & -0.115 & 0.72\end{bmatrix}\ . \tag{3.23}$$

The natural and mean-field hole-state orbitals are, to a good approximation, linear combinations of each other. This implies that (i) the nondiagonal elements $\langle\phi_{nl}\,|\,\rho\,|\,\phi_{n'l}\rangle$ are of the order of the differences between occupation numbers n_{nl} of natural orbitals for hole states, and (ii) the n_{nl} for hole states can be estimated approximately by diagonalizing the density matrix in the subspace of mean-field hole states. For example, by diagonalizing the matrix (3.23) we obtain $n_{10}\simeq 0.54$ (0.54), $n_{20}\simeq 0.62$ (0.63), and $n_{30}\simeq 0.82$ (0.85), where the exact values from Table IV are given in parentheses.

The localized mean-field orbitals are similar in spirit to the Wannier functions in solid-state physics.[6] It should be noted here that the density matrix $\rho(\mathbf{r},\mathbf{r}')$ is the short-

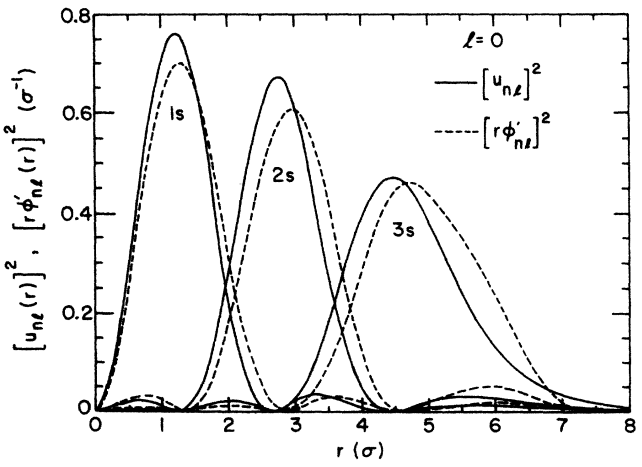

FIG. 9. The $1s$, $2s$, and $3s$ natural (solid lines) and localized mean-field (dashed lines) orbitals in the 70-particle liquid ^{3}He drop. The figure shows $(u_{nl})^2$ and $(r\phi_{nl}')^2$.

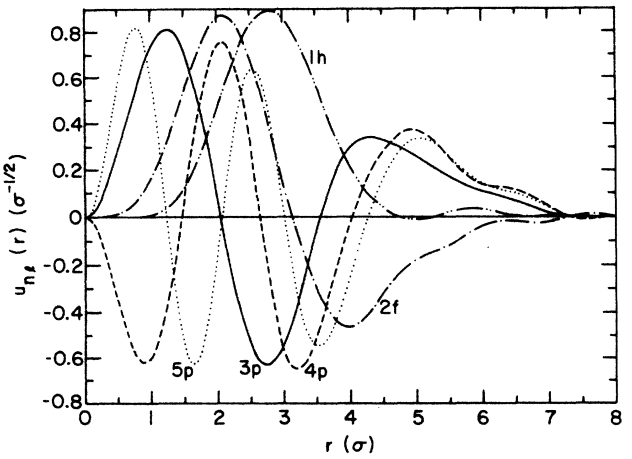

FIG. 10. Some natural particle-state orbitals of the 70-particle liquid ^{3}He drop. The figure shows u_{nl}.

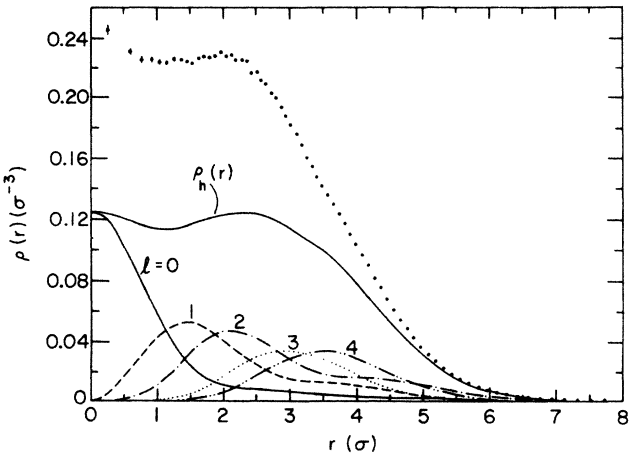

FIG. 11. The partial contribution of hole-state natural orbitals to the density $\rho_h(r)$ compared with the total $\rho(r)$ (error bars) of the $N=70$ ^{3}He drop. The curves labeled 0 to 4 show contributions of hole states with $l=0$ to 4.

time limit of the one-particle Green's function:[7]

$$\rho(\mathbf{r},\mathbf{r}')=\langle N \mid a^+(\mathbf{r})a(\mathbf{r}') \mid N\rangle \tag{3.24}$$

$$=-i\lim_{\varepsilon\to 0^+} G(\mathbf{r}',t'=t-\varepsilon;\mathbf{r},t)\ , \tag{3.25}$$

where $\mid N\rangle$ is the N-particle ground state and $a(\mathbf{r})$ destroys a particle at position $\mathbf{r}$. It thus involves a sum over all frequencies, and hence it is not surprising that the single-particle wave functions which offer a most convenient representation of $\rho(\mathbf{r},\mathbf{r}')$ are not eigenstates of the mean-field Hamiltonian.

The natural orbitals for hole states are not very sensitive to the details of the correlations in the wave function. They are unaffected by the three-body and backflow correlations. It appears that a small amount of pair correlation is sufficient to give localized natural orbitals. For example, calculations carried out with the McMillan pair correlation,

$$f_2(r)=\exp[-\tfrac{1}{2}(b/r)^5]\ , \tag{3.26}$$

give localized natural orbitals even for b as small as 0.5σ. The typical value of b in liquid ^{3}He at equilibrium density is 1.17σ.

TABLE V. Number of particles having a given angular momentum for the 70-atom ^{3}He drop.

l	N_l (hole)	N_l (particle)	N_l (total)
0	4.04	0.29	4.33
1	8.06	0.98	9.04
2	14.28	1.38	15.67
3	9.65	2.05	11.69
4	13.46	2.00	15.46
5		2.59	2.59
6		2.38	2.38
7		1.85	1.85
8		1.40	1.40
9		0.99	0.99
10	—	0.83	0.83
Total	49.49	16.74	66.23

Some of the natural particle orbitals, which are occupied with small probabilities (Table IV), are shown in Fig. 10. They have the conventional number of radial nodes, and are confined to the region where $\rho(r)\neq 0$. The number of atoms in hole and particle orbitals of a given l are shown in Table V, from which we find that $\sim 70\%$ of the atoms are in hole states. The partial contributions of the hole-state natural orbitals to the density are shown in Fig. 11, where $\rho_h(r)$ is the sum of all hole-state contributions to the $\rho(r)$. As expected, near the center of the drop, particles in the hole orbitals account for only $\sim\frac{1}{2}$ of the total density, whereas at the surface they give a more dominant contribution.

IV. MOMENTUM DISTRIBUTION

A. Calculation of momentum distribution

The $\tilde{\rho}(\mathbf{k})$ of Eq. (1.8) can be directly evaluated as

$$\tilde{\rho}(\mathbf{k})=\frac{N}{(2\pi)^3}\int\int \Psi_v^*(\mathbf{r}_1',\tau_1')e^{i\mathbf{k}\cdot(\mathbf{r}_1'-\mathbf{r}_1)} \times\Psi_v(\tau)d^3r_1'\,d\tau\Big/\int \mid\Psi_v(\tau)\mid^2 d\tau\ . \tag{4.1}$$

As in Sec. III A, the spherical symmetry of the drops being considered here allows us to simplify this to

$$\tilde{\rho}(\mathbf{k})=\tilde{\rho}(k) =\frac{N}{2\pi^2}\int \mid\Psi_v(\tau)^2 \times\left[\int\frac{\Psi_v(\mathbf{r}_1',\tau_1')}{\Psi_v(\tau)}J_0(k\mid\mathbf{r}_1'-\mathbf{r}_1\mid) \times(r_1')^2dr_1'\right]d\tau\Big/\int\mid\Psi_v(\tau)\mid^2 d\tau\ , \tag{4.2}$$

where $\mathbf{r}_1'$ is oriented in an arbitrary fixed direction.

The integral over τ was again done by Monte Carlo sampling, and the one-dimensional integral over r_1' was done at each configuration by using 24 Gauss-Legendre quadrature points. The inner integral was evaluated separately for particles $1,2,\ldots,N$ and the results averaged to obtain better statistics. Only one direction of $\mathbf{r}_1'$ ($\hat{\mathbf{r}}_1'=\hat{\mathbf{z}}$) was used.

B. Momentum distribution in Bose-liquid ^{4}He drops

We have calculated the momentum distributions in Bose-liquid ^{4}He drops containing 20–240 atoms. Some of the results are shown in Figs. 12 and 13. Figure 12, for $N=70$, also shows that the $\tilde{\rho}_{MF}(k)$ obtained from the mean-field wave function does not give a good description of $\tilde{\rho}(k)$. The structure of $\tilde{\rho}(k)$ at small k is similar to that of $\tilde{\rho}_{MF}(k)$; hence, we can attempt to fit $\tilde{\rho}(k)$ as

$$\tilde{\rho}(k)=Q\tilde{\rho}_{MF}(k)+B(k)\ , \tag{4.3}$$

insisting that the background $B(k)$ is smooth and does not have any structure at small k. Such fits are not very good (Fig. 12) because the first peak, at $k=0$, of the $\tilde{\rho}_{MF}(k)$ is a little too wide, and the second peak is too small and at too large k. The factor Q obtained from such a fit has to be interpreted as the fraction of particles in the condensate. In fact, $N\times Q$ is systematically larger than the number of particles in the condensate determined in Sec. III from natural orbitals. For example, in the 70-atom drop, $n_{1s}=25.3$, whereas $N\times Q=33.5$.

A simple and much more accurate explanation of $\tilde{\rho}(k)$ in liquid ^{4}He drops is obtained by using the momentum distribution $|\tilde{\psi}_{1s}(\mathbf{k})|^2$ of the $1s$ natural orbital. The $\tilde{\rho}(k)$ can be expressed as

$$\tilde{\rho}(k)=n_{1s}\,|\tilde{\psi}_{1s}(\mathbf{k})|^2+B(k)\ , \tag{4.4}$$

and we can use the Fourier transform of the LDA $\psi_{1s}(r)$ [Eq. (3.11)] for calculating the $\tilde{\psi}_{1s}(\mathbf{k})$. The fits obtained with Eq. (4.4) are almost perfect (Fig. 13), and the values of n_{1s} obtained by fitting the $\tilde{\rho}(k)$ are accurate. For example, the n_{1s} obtained from Eq. (4.4) is 26.1 against 25.3 found in Sec. III by diagonalizing the density matrix. Thus all of the structure in $\tilde{\rho}(k)$ for small k is described by the $1s$ natural orbital. As will be seen in Sec. V, this is effectively the same as the quasihole orbital. The condensate fractions (n_{1s}/N) obtained by various means are given in Table VI.

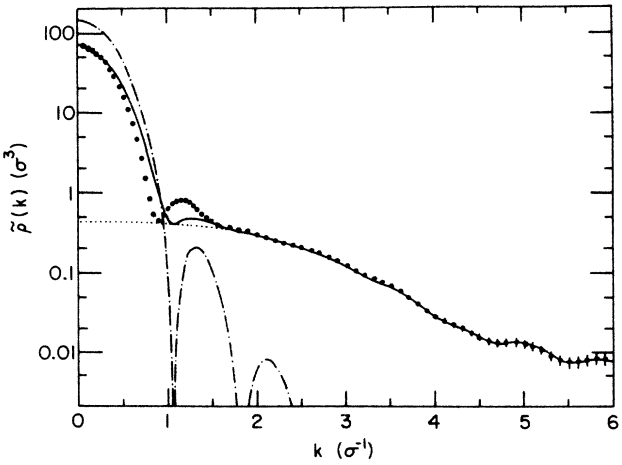

FIG. 12. The $\tilde{\rho}(k)$ (data points) and $\tilde{\rho}_{MF}(k)$ (dot-dash) of the $N=70$ ^{4}He drop. The solid curve shows $0.48\tilde{\rho}_{MF}(k)+B(k)$, and the background $B(k)$ is shown by the dotted line.

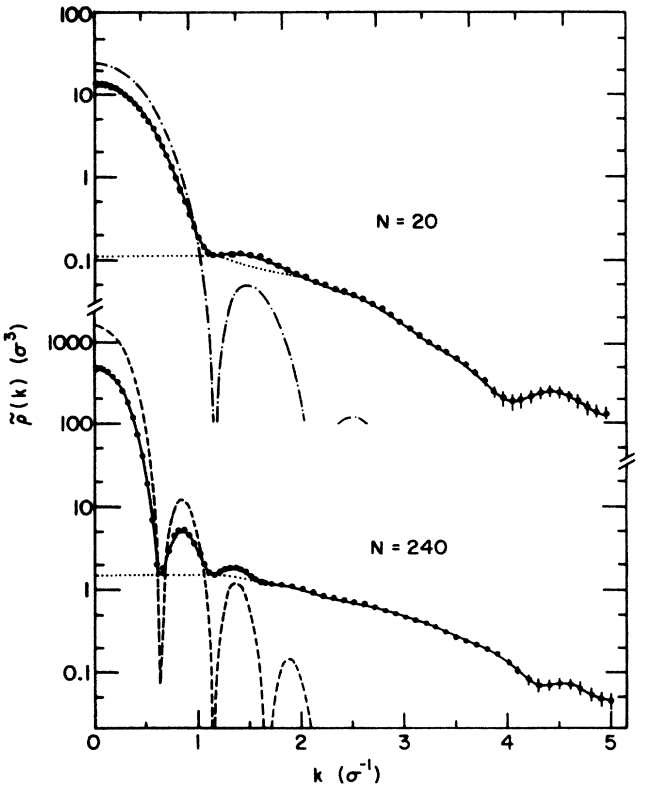

FIG. 13. The $\tilde{\rho}(k)$ (data points) and $N\,|\tilde{\psi}_{1s}(\mathbf{k})|^2$ (dot-dash) in the $N=20$ (upper) and $N=240$ (lower) ^{4}He drops. The solid curve shows $n_{1s}\,|\tilde{\psi}_{1s}(k)|^2+B(k)$, and the background $B(k)$ is shown by the dotted line.

The contributions of particles in the condensate and other natural orbitals to the $\tilde{\rho}(k)$ of the $N=70$ Bose-liquid ^{4}He drop are shown in Fig. 14. The sum of the contributions of all particles having $l\le 10$ is compared with the total $\tilde{\rho}(k)$. We see that particles having $l>10$ contribute mostly to $\tilde{\rho}(k)$ for $k>4\sigma^{-1}$.

The momentum distribution per atom $[\tilde{\rho}(k)/N]$ of the $N=20$, 70, and 240 drops is compared with that of extended liquid ^{4}He in Fig. 15. The $\tilde{\rho}(k)/N$ for $k>1.5\sigma^{-1}$

TABLE VI. Estimates of the condensate fraction of Bose-liquid drops. The columns give the values obtained from $\rho_l(r,r')$ eigenvalues (DM), Eq. (3.24) (LDA), Eq. (4.4) (MD) and Eq. (5.1) (Z).

N	DM	LDA	MD	Z
20		0.49	0.55	0.52±0.02
70	0.36	0.37	0.37	0.35±0.02
240		0.29	0.29	0.29±0.02

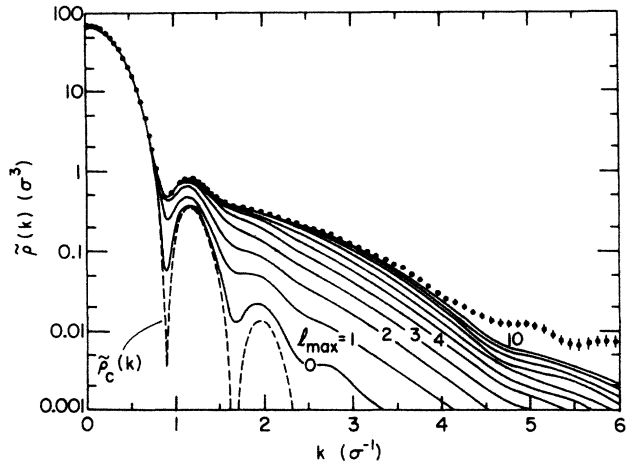

FIG. 14. The $\tilde{\rho}(k)$ of the $N=70$ ^{4}He drop (data points), $\tilde{\rho}_c(k)$ (dashed line), and summed partial contributions for $0 \le l \le l_{max}$ (solid curves).

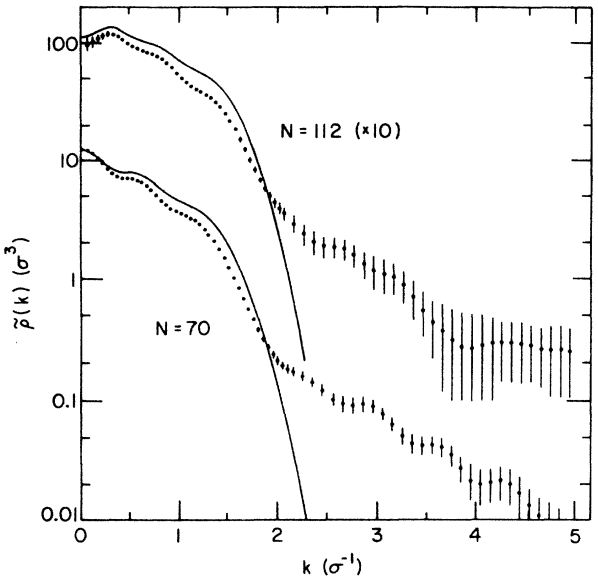

FIG. 16. The $\tilde{\rho}(k)$ (error bars) and $\tilde{\rho}_{MF}(k)$ (solid curves) in the 70- and 112- atom ^{3}He drops.

does not have a large dependence upon N when $N \gtrsim 20$. At large k the $\tilde{\rho}(k)/N$ increases as N increases from 20 to ∞. We note that the kinetic energy per atom[1] in $N=20$, 70, 240, and ∞ systems is, respectively, 4.4, 7.0, 8.7, and 14.7 K.

C. Momentum distribution in Fermi-liquid ^{3}He drops

The $\tilde{\rho}(k)$ of Fermi-liquid ^{3}He drops with 70 and 112 atoms is compared with the $\tilde{\rho}_{MF}(k)$ in Fig. 16. Both the $\tilde{\rho}(k)$ and $\tilde{\rho}_{MF}(k)$ have a rather sharp drop at $k \sim 2\sigma^{-1}$, which is close to the value of k_F ($2.02\sigma^{-1}$) of liquid ^{3}He at equilibrium density. At smaller values of k ($<2\sigma^{-1}$), the $\tilde{\rho}(k)$ is smaller than the $\tilde{\rho}_{MF}(k)$ by $\sim 20\%$ in these drops. In contrast, in the extended liquid for $k < k_F$, $\tilde{\rho}(k)/N \sim 0.5$, while $\tilde{\rho}_{MF}(k)/N = 1$. At larger values of k the $\tilde{\rho}(k)$ is much larger than the $\tilde{\rho}_{MF}(k)$, as expected.

The contributions, as computed from the $\tilde{\psi}_{nl}(k)$, of various angular momenta to the $\tilde{\rho}(k)$ of the $N=70$ drop are shown in Fig. 17. We note that the contributions from $l \le 10$ states account for most of the $\tilde{\rho}(k)$ except at very small and large momenta. The differences at small k are probably due to difficulties in numerically extracting the $\tilde{\rho}_l(k \to 0)$ from natural orbitals, whereas the $\tilde{\rho}(k)$ at large k should have contributions from natural orbitals having $l > 10$. We note that the number of particles in orbitals having $l \le 10$ is estimated to be 66.2 in the

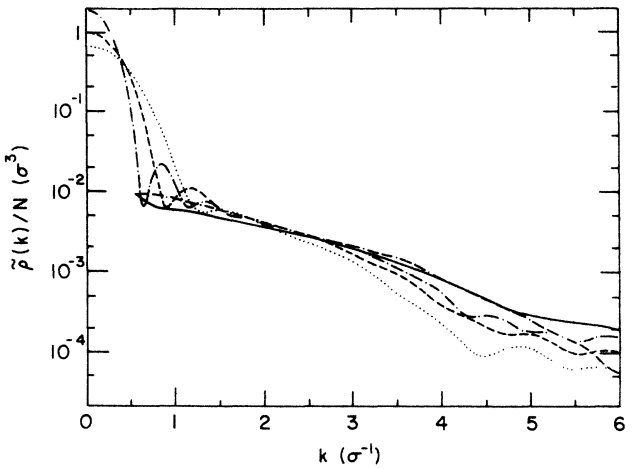

FIG. 15. The $\tilde{\rho}(k)/N$ of $N=20$ (dotted), 70 (dashed), and 240 (dot-dash) drops, compared with that of the extended liquid as estimated from experimental (Ref. 9) (dash-dash-dot), and variational calculations (Ref. 4) (solid). The Green's-function Monte Carlo calculations (Ref. 11) also give a very similar $\tilde{\rho}(k)/N$ for extended liquid ^{4}He.

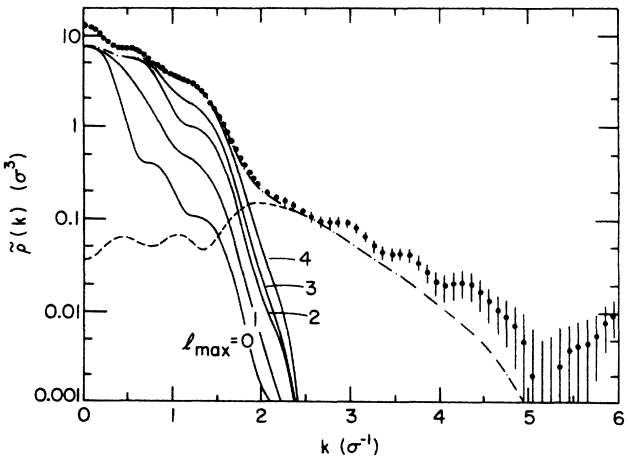

FIG. 17. The $\tilde{\rho}(k)$ (error bars) for the 70-atom ^{3}He drop and natural-orbital contributions. The solid curves show the sum up to the indicated l_{max} of the hole orbitals. The dashed curve is the sum up to $l=10$ of all the particle orbitals. The dot-dash curve is the sum of all natural orbitals up to $l=10$.

present calculation.

The calculated $\tilde{\rho}(k)/N$ in $N=40$, 70, and 112 drops is compared with the momentum distribution (per atom) in liquid ^{3}He in Fig. 18. The $\tilde{\rho}(k)/N$ in the drops is much larger than that in liquid at small k, and it is somewhat smaller at large k. The total kinetic energy per particle is 3.9, 5.1, 5.8, and 12.3 K in systems having $N=40$, 70, 112, and ∞, respectively.[1] Note that at large values of k there are significant statistical sampling errors are indicated in Fig. 16.

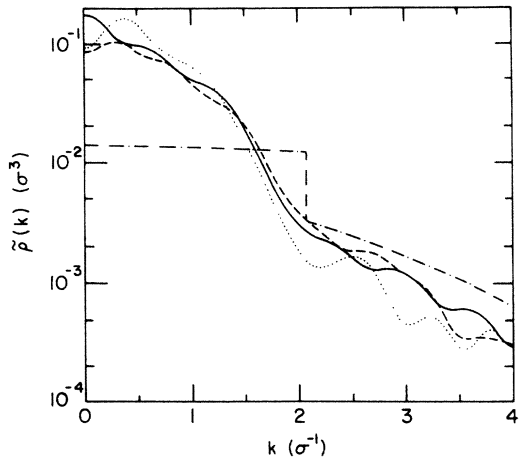

FIG. 18. $\tilde{\rho}(k)/N$ for the 40-atom (dotted), 70-atom (solid), and 112-atom (dashed) ^{3}He drops. The dot-dash curve is for the infinite liquid (Ref. 5).

V. QUASIHOLE WAVE FUNCTIONS

A. Calculation of quasihole wave functions

In Bose-liquid drops the only quasihole state is the $1s$ state; its wave function χ_{1s} is calculated from the expression

$$\chi_{1s}(\mathbf{r}_1)=\frac{1}{\sqrt{Z}}\frac{\int \Psi^*_{N-1}(\tau'_1)\Psi_N(\tau)d\tau'_1}{\left[\int |\Psi_{N-1}(\tau'_1)|^2 d\tau'_1\right]^{1/2}\left[\int |\Psi_N(\tau)|^2 d\tau\right]^{1/2}}, \tag{5.1}$$

where Ψ_{N-1} and Ψ_N are the ground states of the N and $N-1$ particle drops, and Z is the normalization constant determined from

$$\int \chi^2_{nl}(\mathbf{r})d^3r=1 . \tag{5.2}$$

In practice we calculate the Fourier-Bessel transforms of χ_{1s} using the following equations:

$$\tilde{\chi}_{1s}(\mathbf{k})=\sqrt{Y/Z}\,\bar{\chi}_{1s}(k) , \tag{5.3}$$

$$\bar{\chi}_{1s}(\mathbf{k})=\frac{1}{N}\sum_{i=1,N}\frac{\int \Psi^*_{N-1}(\tau'_i)j_0(kr_i)\Psi_N(\tau)d\tau}{\int |\Psi_N(\tau)|^2 d\tau} , \tag{5.4}$$

$$Y=\int \frac{\int |\Psi_N(\tau)|^2 d\tau'_1}{\int |\Psi_{N-1}(\tau'_1)|^2 d\tau'_1} d^3r_1 . \tag{5.5}$$

The $\tilde{\chi}_{1s}(k)$ are calculated by Monte Carlo integration. The integration over $d\tau'_1$ in Y is done by the Monte Carlo method, while that over d^3r_1 is done by Gauss-Legendre quadrature. As is the case in Secs. III and IV, the spherical symmetry reduces this integral to a radial integral.

The variational wave functions of Ref. 1 are used to approximate the $\Psi_N(\tau)$. The $\Psi_{N-1}(\tau'_i)$ has the same form as that of Ψ_N. The triplet- and pair-correlation functions f_3 and f_2 have a very small dependence on N, and hence they are taken to be the same as in Ψ_N. The single-particle function f'_1, in the $N-1$ particle drop is taken as

$$f'_1(r)=f_1(r+s) , \tag{5.6}$$

$$s=0.46[N^{1/3}-(N-1)^{1/3}]\sigma , \tag{5.7}$$

where $f_1(r)$ is the one-particle function in Ψ_N. Equations (5.6) and (5.7) take into account the smaller size of the $N-1$ particle drop. The coefficient 0.46σ in Eq. (5.7) is obtained by fitting the dependence of f_1 on N. The shift s is rather small, and has little effect on the results. It is a good approximation to take f'_1 in the $N-1$ particle drop to be the same as f_1 in the N-particle drop.

We have studied the quasihole wave functions in the $N=70$ Fermi-liquid ^{3}He drop. This drop has a closed-shell structure, and we do not expect it to have many particle-hole-type excited states at energies less than $2\omega_s$, where ω_s (~ 0.8 K from Fig. 1) is the spacing between shells. The $N=69$ drop is expected to have three almost degenerate low-energy states (one of which, presumably the $3s$, is the ground state). These three states can be thought of as the single-hole states, and the quasihole wave functions χ_{nl} for $nl=3s$, $2d$, and $1g$ can be obtained from them:

$$\chi_{nl}(r_1)=\sqrt{Y_{nl}/Z_{nl}}\,\frac{\int \Psi^*_{N-1}[(n,l,m,s)^{-1},\tau'_1]Y^*_{lm}(\hat{\mathbf{r}}_1)\Psi_N(\tau)d\tau'_1 d\hat{\mathbf{r}}_1}{\int |\Psi_N(\tau)|^2 d\tau} . \tag{5.8}$$

The wave function $\Psi_{N-1}[(n,l,m,s)^{-1},\tau_1']$ of the hole state is approximated by Eq. (1.12).

In practice, Eq. (5.9) can be used to calculate the $\chi_{nl}(r)$ for all the hole states. However, the $1s$, $1p$, $2s$, and $1d$ hole states are at energies of $\sim 3\omega_s$ at which we can have a large density of one-particle two-hole states. Thus the single-hole states would mix with them and acquire large widths. In general, the wave function $\Psi_{N-1}[(n,l,m,s)^{-1}]$ is not expected to be a good approximation for any state of the $N-1$ particle drop when nl corresponds to a $3\omega_s$ or more excitation. If these problems are ignored, and the above equations are used to calculate the χ_{nl} for these high-energy hole states, it is found that χ_{1s}, χ_{2s}, and χ_{3s} are not orthogonal to each other; similarly, χ_{1d} is not orthogonal to χ_{2d}, etc. However, we may use Eqs. (5.8) and (1.12) to calculate the wave functions χ_{2p} and χ_{1f} with marginal justification without facing orthogonality problems.

In Fermi-liquid drops, both Z and Y depend upon the orbital quantum numbers n and l. We have not calculated the normalizations Y for the Fermi case, and only the ratio Y/Z is determined by normalizing the χ_{nl}.

B. The quasihole wave function in Bose-liquid drops

The Fourier-Bessel transform of the quasihole wave function χ_{1s} in the $N=240$ Bose-liquid ^{4}He drop is shown in Fig. 19 along with that of the natural orbital ψ_{1s} calculated in the LDA [Eq. (3.11)]. We see that in this case, and also in all the cases we have studied ($N=20$, 40, 70, 112, and 240), the χ_{1s} is very close to the ψ_{1s} in Bose-liquid drops. This is because almost all of the s-wave natural-orbital occupation is in the $1s$ orbital (Table III). To see this, we express $\chi_{1s}(r)$ in terms of the notation introduced in Eq. (3.24):

$$\chi_{1s}(\mathbf{r})=\frac{1}{\sqrt{NZ}}\langle N-1\,|\,a(\mathbf{r})\,|\,N\rangle\ , \tag{5.9}$$

and consider the coefficients of an expansion of $\chi_{1s}(r)$ in terms of the s-wave natural orbitals:

$$q_n=\int \psi_{ns}^*(r)\chi_{1s}(r)r^2dr \tag{5.10}$$

$$=\frac{1}{\sqrt{NZ}}\int \psi_{ns}^*(\mathbf{r})\langle N-1\,|\,a(\mathbf{r})\,|\,N\rangle d^3r\ . \tag{5.11}$$

By inserting a sum over all eigenstates $|N-1,\alpha\rangle$ of the $N-1$ particle system in Eq. (3.24) and using Eq. (3.6), we obtain

$$\sum_\alpha \left|\int \psi_{ns}^*(r)\langle N-1,\alpha\,|\,a(r)\,|\,N\rangle d^3r\right|^2=n_{ns}\ , \tag{5.12}$$

and thus

$$|\,q_n\,|\le[n_{ns}/(NZ)]^{1/2}\ . \tag{5.13}$$

However, the normalization of $\chi_{1s}(r)$ requires that

$$\sum_n |\,q_n\,|^2=1\ , \tag{5.14}$$

and, because NZ is not small while the n_{ns} for $n>1$ are small, we see that q_1 must be nearly unity, and $NZ\sim n_{1s}$.

Since $\chi_{1s}(r)\sim\psi_{1s}(r)$, the LDA [Eq. (3.16)] implies that the ratio $\chi_{1s}(r)/\sqrt{\rho(r)}$ is proportional to $\sqrt{n_0[\rho(r)]}$. The ratio $\chi_{1s}(r)/\sqrt{\rho(r)}$, normalized to 0.907 at $\rho=0.137\rho_0$, is shown as a function of ρ in Fig. 6. Ideally, this ratio would be normalized to unity at $\rho=0$. However, sampling errors make this impracticable so we used the above normalization point. We note that for $N=20$, 70, and 240 this ratio is consistent with the LDA.

The fraction of particles in the condensate, as estimated from (i) diagonalizing the one-particle density matrix, (ii) LDA [Eq. (3.17)], (iii) fits to the momentum distribution by Eq. (4.4), and (iv) the normalization Z calculated by Eqs. (5.1)–(5.5), are shown in Table VI. These estimates are in good agreement with each other. In particular, the agreement of the values of Z with the other estimates of n_{1s}/N suggests that the ground state of the $N-1$ particle drop is reached by removing a particle from the condensate of the N-particle drop, when $N\gtrsim 20$.

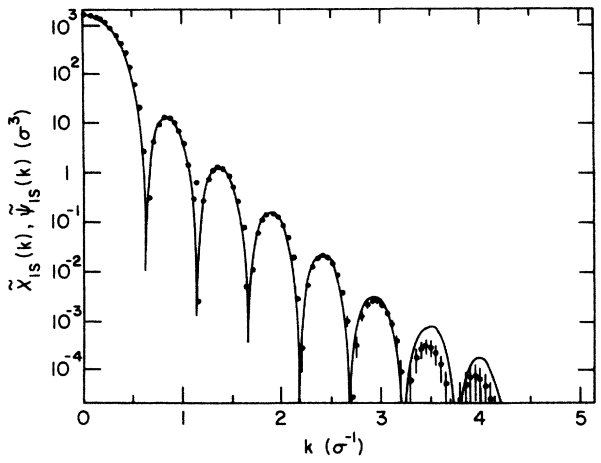

FIG. 19. The $\tilde{\chi}_{1s}(k)$ (error bars) and the LDA for $\tilde{\psi}_{1s}(k)$ (solid curve) for the 240-atom ^{4}He drop.

C. Quasihole wave functions of Fermi-liquid ^{3}He drops

The χ_{nl} for $nl=3s$, $2d$, $1g$, $2p$, and $1f$ states are shown along with the mean-field ϕ_{nl} and natural ψ_{nl} in Figs. 8 and 20. In these figures we show that the LDA,

$$\chi_{nl}(r)\simeq[1-0.45\rho(r)/\rho_0]\phi_{nl}(r)/\sqrt{Z_{nl}}\ , \tag{5.15}$$

provides a good description of the quasihole wave functions. The renormalization constant $Z(\rho)$ in liquid ^{3}He is given by

$$Z(\rho)=\lim_{\varepsilon\to 0^+}[n(k_F-\varepsilon)-n(k_F+\varepsilon)]\ , \tag{5.16}$$

as shown by Migdal.[10] It has been estimated[5] at $\rho>\rho_0$ from the momentum distribution of atoms in liquid ^{3}He, and it appears that the function $[1-0.45\rho/\rho_0]$ provides an approximate extrapolation of $\sqrt{Z(\rho)}$ as shown in Fig. 6.

The nodeless $1f$ and $1g$ quasihole wave functions are rather close to the natural $1f$ and $1g$ wave functions;

however, the $2p$, $2d$, and $3s$ quasihole wave functions are different from both the mean-field wave functions and natural orbitals. Let us consider the $l=0$ wave functions. We may expand χ_{3s} in terms of the ψ_{ns} in the same manner as was done for the boson case in Sec. V B. However, for the Fermi case, the occupation numbers of the $1s$, $2s$, and $3s$ orbitals are comparable, and hence there are at least three significant terms in the expansion. Thus, in general, quasiparticle orbitals are not equal to natural orbitals, the exception being $n=1$ states that are near the Fermi energy. Since the quasihole orbitals are in between the natural and mean-field orbitals, their occupation numbers $\langle \chi_{nl} | \rho | \chi_{nl} \rangle$ are also in between the natural n_{nl} and $\langle \phi_{nl} | \rho | \phi_{nl} \rangle$ as shown in Table VII.

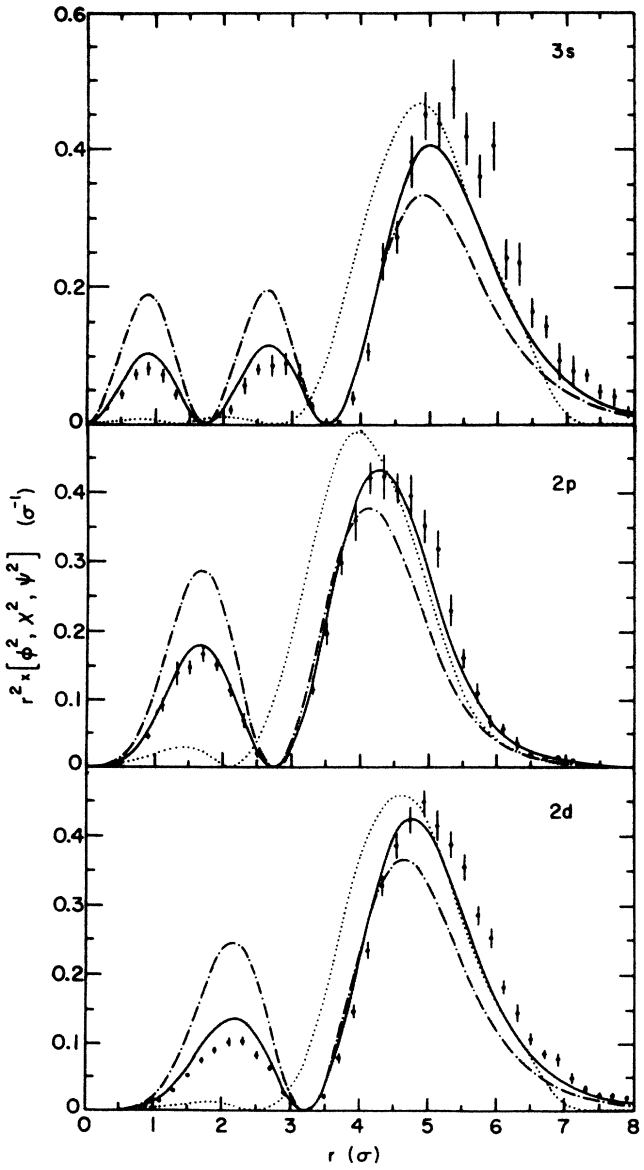

FIG. 20. Same as Fig. 8 except for the $3s$ (upper), $2p$ (middle), and $2d$ (lower) orbitals.

TABLE VII. Occupation numbers of natural, quasihole, and mean-field orbitals.

n,l	$n_{n,l}$	$\langle \chi_{n,l} \mid \rho \mid \chi_{n,l} \rangle$	$\langle \phi_{n,l} \mid \rho \mid \phi_{n,l} \rangle$
$3s$	0.85	0.76	0.72
$2d$	0.84	0.77	0.74
$1g$	0.75	0.74	0.74
$2p$	0.77	0.72	0.71
$1f$	0.69	0.69	0.69

VI. CONCLUSIONS AND DISCUSSION

One of the main conclusions of this work is that in finite systems the mean-field, natural, and quasiparticle orbitals are generally different. These orbitals will not be identical in any inhomogeneous system such as electrons in a crystal lattice. Only in homogeneous liquids are all these orbitals plane waves, and the theory is simpler.

The main advantage of mean-field wave functions is that they are easy to calculate from the experimental density distribution $\rho(r)$, if it is known, or from a reasonable energy-density functional,[12,13] if that is known. It seems that the quasiparticle wave functions can be obtained with reasonable accuracy from the mean-field wave functions with LDA's such as those given here. The two-particle distribution function can also be obtained from $\rho(r)$ with reasonable accuracy by using a LDA.[14]

We have not investigated the problem of finding a simple way to generate all the natural orbitals from $\rho(r)$ or, equivalently, the $\phi_i(r)$. It appears that if, in the language of mean-field theory, k states with angular momentum l are occupied, then the natural orbitals ψ_{nl} having $n \leq k$ have $k-1$ radial nodes each. When $k>1$, these natural orbitals of the hole states are similar to Wannier-type localized functions formed from the occupied mean-field wave functions. On the other hand, when $k=1$ the hole state ψ_{1l} is similar to the quasiparticle wave function χ_{1l}. The natural orbitals ψ_{nl} of particle states are confined to the region where $\rho(\mathbf{r})>0$. On the other hand, the mean-field ϕ_{nl} are not confined when n or l is large enough so that the orbital energy e_{nl} is positive. Even bound ($e_{nl}<0$) mean-field orbitals for particle states have bigger radii than the corresponding ψ_{nl}. It appears that developing simple methods to estimate the natural orbitals and their occupation probabilities in a quantum-liquid drop is an interesting and challenging problem. This problem has recently received some attention in nuclear physics.[15,16]

The main weakness of this work stems from using the variational wave functions instead of the exact ground state. These wave functions are the best available to date, and comparisons with Green's-function Monte Carlo calculations suggest that they give reasonable binding energies,[1] momentum distributions,[4,5] density distributions,[1] and pair-distribution functions.[17] However, it may be possible to improve upon them by, for example, allowing the pair correlation $f_2(r_{ij})$ to depend upon $\mathbf{r}_i$ and $\mathbf{r}_j$ as suggested by Krotscheck *et al.*[18] The main conclusions of this work, the localization of natural orbitals and the

local-density approximation for the quasiparticle orbitals, are not sensitive to the details of the correlations, and they should exist even when exact ground states are used.

The one-particle Green's function of a finite or inhomogeneous system can be expanded following Lehmann's method,[7,20]

$$G(\mathbf{r},\mathbf{r}',\omega)=G_{\rm qp}(\mathbf{r},\mathbf{r}',\omega)+G_{\rm rest}(\mathbf{r},\mathbf{r}',\omega)\ , \tag{6.1}$$

where $G_{\rm qp}(\mathbf{r},\mathbf{r}',\omega)$ contains the contributions from the quasiparticle states. The single-particle wave functions associated with the quasiparticles are clearly the $\chi_i(\mathbf{r})$, and

$$G_{\rm qp}(\mathbf{r},\mathbf{r}',\omega)=\sum_i \frac{Z_i}{\omega-E_i+E_0+i\eta}\chi_i^*(\mathbf{r})\chi_i(\mathbf{r}') + \sum_j \frac{Z_j}{\omega+E_0-E_j-i\eta}\chi_j^*(\mathbf{r})\chi_j(\mathbf{r}')\ . \tag{6.2}$$

Here E_i and E_j are the energies of quasiparticle states in drops with $N+1$ and $N-1$ particles, respectively.

An expansion of the type (6.2) is generally used to study the response of nuclei[20] and jellium drops,[21] but with the mean-field wave functions ϕ_i instead of the quasiparticle χ_i. The resulting calculated response of nuclei is typically too large at small r where the $\chi_i(r)$ are smaller than the $\phi_i(r)$ (Figs. 8 and 20). Thus, the use of the proper single-particle wave functions may be important in studying the response of small systems.

The density distribution is given by

$$\rho(\mathbf{r})=\lim_{\eta\to 0^+}\int G(\mathbf{r},\mathbf{r},\omega)e^{i\eta\omega}\frac{d\omega}{2\pi}\ . \tag{6.3}$$

Only those poles of $G(\mathbf{r},\mathbf{r}',\omega)$ that are above the real axis contribute to $\rho(\mathbf{r})$. Let us assume that the system with $N-1$ particles has a hole in state j in its ground state. The $G(\mathbf{r},\mathbf{r}',\omega)$ of the $N-1$ particle drop will differ from that of the N-particle drop in two ways. The pole corresponding to the quasiparticle state j will go below the real axis because j is a particle state in the drop having $N-1$ particles, and there will be small changes in the contributions from all other states. If we assume that all these other changes provide a background, then

$$\rho_N(r)-\rho_{N-1}(r)=Z_j\,|\,\chi_j(\mathbf{r})\,|^2+\text{background}\ . \tag{6.4}$$

The volume integral of the background must be $1-Z_j$. If we assume that the background is proportional to $\chi_j^2(\mathbf{r})$, the density difference is given approximately by $|\,\chi_j(\mathbf{r})\,|^2$.

In Fig. 21 we compare the density difference between $N=70$ and $N=69$ liquid ^{3}He drops with $|\,\phi_{3s}\,|^2$ and $|\,\chi_{3s}\,|^2$. We have assumed that the ground state of the $N=69$ drop has $l=0$. In the actual Monte Carlo calculation we removed both $3s$ states from the ϕ_v [Eqs. (1.1) and (1.3)], and measured the $\rho(r)$ of the resulting $N=68$ system. The resulting change in $\rho(r)$ should be close to twice the difference $\rho_{N=70}(r)-\rho_{N=69}(r)$. We see that the density difference produced by the removal of a particle from a closed-shell drop is better described by quasihole rather than mean-field wave functions. The difference is smaller at small r than expected from the mean-field $\phi_{3s}(r)$. Experimentally it is known that the difference between the charge densities of lead and thallium nuclei[22] is smaller than $|\,\phi_{3s}(r)\,|^2$ at $r=0$. A $3s$ proton is removed from lead to reach thallium.

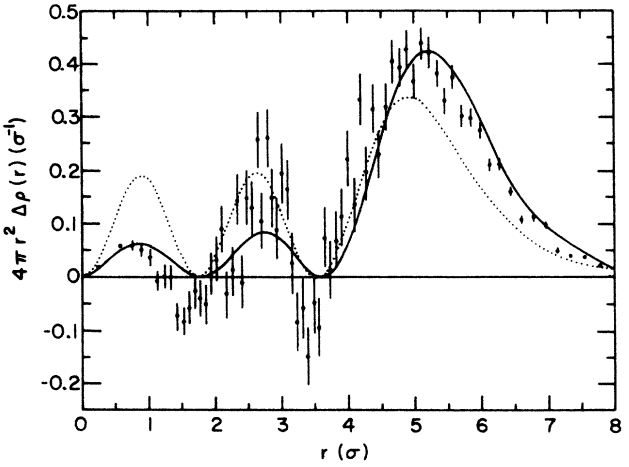

FIG. 21. The estimated density difference $\rho_{N=70}(r)-\rho_{N=69}(r)$ (data points) compared with $|\,\chi_{3s}(r)\,|^2$ and $|\,\phi_{3s}(r)\,|^2$ (dashed curve). The quantity $4\pi r^2\Delta\rho(r)$ is plotted.

ACKNOWLEDGMENTS

The authors thank R. B. Wiringa for useful discussions throughout this work. Two of us (V.R.P.) and (S.C.P.) thank the organizers, G. Bertsch and M. Schluter, of the Workshop on Physics of Small Clusters at the Aspen Center for Physics, for the congenial atmosphere in which much of this work was planned. The calculations were made possible by grants of time on the Energy Research Cray computer of the United States Department of Energy and the Cray computer at the National Center for Supercomputer Applications in Urbana, Illinois. This work is supported by the U.S. Department of Energy (Nuclear Physics Division), under contract No. W-31-109-ENG-38, and by the U.S. Department of Energy (Materials Science Division), under Contract No. DE-AC02-76ER01198, and by the National Science Foundation, Grants No. PHY-84-15064 and No. DMR-83-16981.

[1]V. R. Pandharipande, S. C. Pieper, and R. B. Wiringa, Phys. Rev. B **34**, 4571 (1986).
[2]P.-O. Lowdin, Phys. Rev. **97**, 1474 (1955).
[3]S. Stringari, Phys. Lett. **107A**, 36 (1985).
[4]E. Manousakis, V. R. Pandharipande, and Q. N. Usmani, Phys. Rev. B **31**, 7022 (1985).
[5]J. Carlson, R. M. Panoff, K. E. Schmidt, P. A. Whitlock, and M. H. Kalos, Phys. Rev. Lett. **55**, 2367 (1985); A. Fabrocini

and V. R. Pandharipande, Phys. Rev. B (to be published).
[6]E. I. Blount, *Advances in Solid State Physics,* edited by F. Seitz and D. Turnbull (Academic, New York, 1962), Vol. 13, p. 305.
[7]A. L. Fetter and J. D. Walecka, *Quantum Theory of Many-Particle Systems* (McGraw-Hill, New York, 1971).
[8]D. S. Greywall, Phys. Rev. B **27**, 2747 (1983).
[9]V. F. Sears, Phys. Rev. B **28**, 5109 (1983); (private communication).
[10]A. B. Migdal, Zh. Eksp. Teor. Fiz. **32**, 399 (1957) [Sov. Phys.—JETP **5**, 333 (1957)].
[11]P. A. Whitlock and R. M. Panoff (unpublished).
[12]J. W. Negele, Rev. Mod. Phys. **54**, 913 (1982).
[13]P. Hohenberg and W. Kohn, Phys. Rev. **136**, B864 (1964).
[14]S. C. Pieper, R. B. Wiringa, and V. R. Pandharipande, Phys. Rev. B **32**, 3341 (1985).
[15]M. Jaminon, C. Mahaux, and H. Ngo, Nucl. Phys. A **440**, 228 (1985).
[16]B. L. Friman, in *Proceedings of the International Conference on Unified Concepts of Many-Body Problems, Stony Brook, New York,* edited by J. Speth and T. Kuo (North-Holland, Amsterdam, 1986), p. 41.
[17]R. Schiavilla, D. S. Lewart, V. R. Pandharipande, S. C. Pieper, R. B. Wiringa, and S. Fantoni, Nucl. Phys. **A473**, 267 (1987).
[18]E. Krotscheck, G.-X. Qian, and W. Kohn, Phys. Rev. B **31**, 4245 (1985).
[19]A. B. Migdal, *Theory of Finite Fermi Systems and Applications to Atomic Nuclei* (Interscience, New York, 1968).
[20]D. Gogny, *Nuclear Physics with Electromagnetic Interactions,* Vol. 108 of *Lecture Notes in Physics,* edited by H. Arenhövel and D. Drechsel (Springer-Verlag, New York, 1979), p. 88; D. Goute *et al.*, Phys. Rev. Lett. **45**, 1618 (1980); J. Heisenberg *et al.*, Phys. Rev. C **25**, 2292 (1982).
[21]W. Ekardt, Phys. Rev. Lett. **52**, 1925 (1984).
[22]J. M. Cavedon *et al.*, Phys. Rev. Lett. **49**, 978 (1982).